Studies of Langmuir−Blodgett Films of an Ion Pair Metal Complex Containing Eu(III)-Ru(II) Dual Chromophores

Li-Hua Gao,[†,‡] **Ke-Zhi Wang,**[*,†] **Li Cai,**[⊥] **Hao-Xu Zhang,**[d] **Lin-Pei Jin,**[†] **Chun-Hui Huang,**[§] **and Hong-Jun Gao**[⊥]

Department of Chemistry, Beijing Normal University, Beijing 100875, P. R. China, School of Chemical and Environment Engineering, Beijing Technology and Business University, Beijing 100037, China, State Key Laboratory of Rare Earth Materials Chemistry and Applications and the University of Hong Kong Joint Laboratory on Rare Earth Materials and Bioinorganic Chemistry, Peking University, Beijing 100871, P.R. China, and Beijing Laboratory of Vacuum Physics, Chinese Academy of Science, P.O. Box 2724, P.R. China

A surfactant ion-pair complex, [Ru(bpy)$_2$L][Eu(NTA)$_4$]$_2$ (in which L = 1-docosyl-2-(2- pyridyl)benzimidazole, bpy = 2,2′-bipyridine, and NTA = 4,4,4-trifluoro-1-(2-naphthyl)-1,3-butanedionato) has been synthesized. The surface pressure−area isotherm measurements show that the complex forms a stable Langmuir film at the air−water interface without adding any electrolytes into the subphase. The monolayers formed at the surface pressures of 5 mN m^{-1} and 20 mN m^{-1}, have been successfully transferred onto glass and quartz substrates with the transfer ratios close to unity. The Langmuir−Blodgett films were studied by UV−visible, infrared, and emission spectroscopies, atomic force microscopy, and cyclic voltammetry. The optical, redox, and morphology properties of the LB films were found to be significantly affected by the target surface pressures used for the film depositions.

Introduction

Over the last 40 years, Ru(II) polypyridyl complexes have attracted tremendous interest as photosensitizers for conversions of solar energy into chemical or electrical energy,[1] photocatalytic reduction of carbon dioxide,[2] and oxidation of water to hydrogen and oxygen,[3] and as active components for intelligent sensing and switching devices,[4] and electrogenerated chemiluminescent and electroluminescent devices.[5] All of these applications were based on electron or/and energy transfer reactions performed by photoinduced excited or electrically excited Ru(II) polypyridyl compounds. Usually, directional photoinduced electron or/and energy transfers in fluid solutions are not desirable because back processes with redox couples are difficult to suppress. The Langmuir−Blodgett (LB) technique[7,8] is one of the powerful approaches of making well organized molecular assemblies with precisely controlled thickness at the molecular level, crucial to performing efficient energy transfers, which are far removed from the random molecular arrangements in solution.

To date many Ru(II) complexes have been introduced into LB films.[9−19] These films have shown interesting optical and redox properties,[9−19] and found widespread applications in second-order nonlinear optics,[12] heterogeneous catalysis,[13] photovoltaic devices and photoenergy conversion cells,[14] chemical and biological sensors,[15] energy transfer and electron-transfer devices,[16] modified electrodes for electrolysis and electrogenerated chemiluminescence,[17] gas sensor,[18] and the synthesis of supramolecular complexes via interface coordination reactions.[19] On the other hand, Eu(III) β-diketonates exhibit intriguing *f−f*

emission characteristics, line-like narrow bandwidths (typically a few nanometers), high emission efficiency and relatively long luminescent lifetimes (up to milliseconds), arousing keen interest for photoelectric devices.[20]

We[21−26] and others[27,28] have reported on the LB films of luminescent Eu(III) complexes and found that the photophysical properties of these Eu(III) complexes could be tuned by changing film preparation parameters. We also proved that the use of the hydrophobic and anionic lanthanide β-diketonate could greatly improve the Langmuir and LB film-forming properties of cationic amphiphilics.[29−33] By extending this strategy,[25] here we report on the preparation of an amphiphilic ion pair complex containing two strongly emissive chromophores of a Ru(II) complex cation and an Eu(III) complex anion. We focus our attention on studying Langmuir- and LB-forming properties, and the optical properties of the LB films of the complex containing chromophoric Eu(III) and Ru(II) complexes. The resultant Langmuir film is stable toward solubility and hydrolysis side reactions at the air−water interface; interestingly, each molecular component contributes different luminescent properties to LB films, and the morphology and electrochemical properties of the LB films could be tuned, depending on the surface pressures used for the film depositions. The results provide important fundamental data for the development of novel photoelectronic devices by modulating the optical and electrochemical properties of the composite material containing dual chromophores.

Experimental Section

Materials. 4,4,4-Trifluoro-1-(2-naphthyl)-1,3-butanedione (HNTA) and RuCl$_3$·*n*H$_2$O were purchased from Aldrich. Ru-(bpy)$_2$Cl$_2$·2H$_2$O[34] (bpy = 2,2′-bipyridine) and HDP[Eu-(NTA)$_4$][24] (HDP = *N*-hexadecyl pyridinium, NTA = deprotonated HNTA) were synthesized according to the literature

* To whom correspondence should be addressed. E-mail: kzwang@bnu.edu.cn.
† Beijing Normal University.
‡ Beijing Technology and Business University.
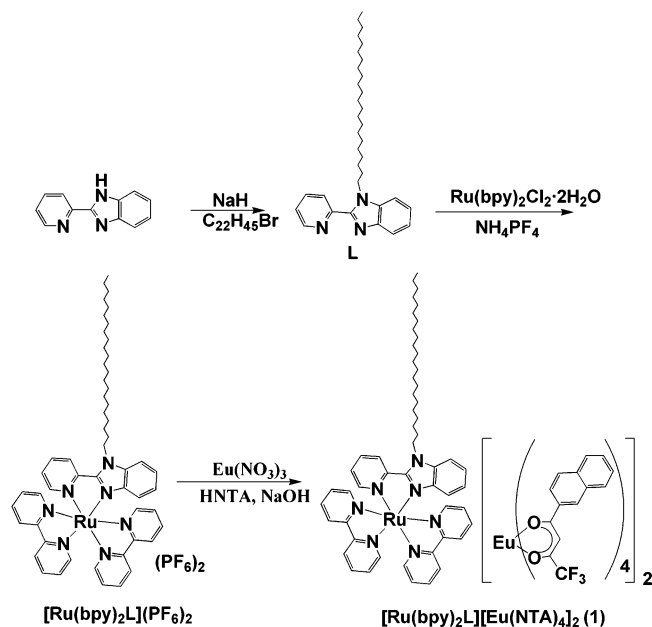§ Peking University.
⊥ Chinese Academy of Science.

Langmuir−Blodegett Film of Ru(II)−Eu(III) dual chromophores

J. Phys. Chem. B, Vol. 110, No. 14, 2006 **7403**

Figure 1. The synthetic route to the ion-pair complex **1**.

methods. The synthetic route to the ion-pair complex, [Ru-(bpy)$_2$L][Eu(NTA)$_4$]$_2$, is shown in Figure 1.

Synthesis of Docosyl-2-(2-pyridyl)benzimidazole (L). This was synthesized according to the procedure described for 2-(1-octadecylbenzimidazol-2-yl)pyridine except that 1-bromo-docosane was used instead of 1-bromooctadecane.[21] The crude product was chromatographed on silica gel with CH$_2$Cl$_2$–CH$_3$OH (9:1, v/v) as an eluant. Yield 68%. M.p. 63−64 °C. Anal. Calcd for C$_{34}$H$_{53}$N$_3$: C, 81.06; H, 10.60; N, 8.34%. Found: C, 80.73; H, 10.55; N, 8.35%. ^{1}H NMR (400 MHz, CDCl$_3$): δ 0.878 (t, 3H, −CH$_3$); 1.30(m, 38H, -(CH$_2$)$_{19}$); 1.88(m, 2H, −CH$_2$); 4.82-(t, 2H, −CH$_2$); 7.33(m, 3H, -ph); 7.45(d, 1H, -ph); 7.84 (m, 2H, -ph); 8.41 (d, 1H, -ph), 8.69 ppm (s, 1H, -ph). IR (KBr): 432(w); 698(w); 717(m);734(vs); 748(m); 795(m); 992(w); 1006(w); 1095(w); 1142(m); 1332(m); 1444(s); 1466(s); 1592-(m); 2846(vs); 2915 cm^{-1} (vs). UV in CHCl$_3$ λ_{max}: 311 nm.

Synthesis of [Ru(bpy)$_2$L](PF$_6$)$_2$. L (0.195 g, 0.39 mmol) and Ru(bpy)$_2$Cl$_2$·2H$_2$O (0.190 g, 0.37 mmol) in degassed ethylene glycol (20 mL) were heated for 24 h under the protection of nitrogen. To the filtered solution was added 4-fold excess of saturated aqueous solution of NH$_4$PF$_6$. The precipitate formed was filtered and twice recrystallized from CH$_2$Cl$_2$−hexane. Anal. Calcd for C$_{54}$H$_{69}$N$_7$RuP$_2$F$_{12}$: C, 53.75; H, 5.72; N, 8.12%. Found: C, 53.62; H, 5.58; N, 8.03%. M.p. 215−216 °C. UV−visible in CHCl$_3$, λ/nm ($\epsilon \times 10^{-4}$/M^{-1} cm^{-1}): 460(1.86); 340-(2.48); 323(3.22); 290(7.86).

Synthesis of [Ru(bpy)$_2$L][Eu(NTA)$_4$]$_2$ (1). A solution of HNTA (0.213 g, 0.8 mmol) in ethanol (20 mL) was neutralized with sodium hydroxide aqueous solution (0.4 mL, 2.0 M). An Eu(NO$_3$)$_3$ aqueous solution (0.2 mL, 1.0 M) was then added under gentle heating and continuous stirring. To this mixture a solution of [Ru(bpy)$_2$L](PF$_6$)$_2$ (121 mg, 0.1 mmol) in ethanol (10 mL) was dropwise added. A mass red precipitate quickly appeared was filtered, washed with hot ethanol and twice recrystallized from CHCl$_3$−ethanol. Anal. Calcd for C$_{166}$H$_{133}$N$_7$F$_{12}$Eu$_2$O$_{16}$Ru: C, 59.64; H, 4.01; N, 2.93%. Found: C, 59.10; H, 4.04; N, 3.11%. M.p. 106−108 °C. IR(KBr): 473-(w); 568(w); 684(m); 750(w); 766(w); 791(s); 844(vw); 867-(vw); 960(vw); 1074(vw); 1134(s); 1184(s); 1197(s); 1299(vs); 1465(m); 1483(m); 1510(s); 1529(s); 1571(m); 1595(s); 1615-

(vs) cm^{-1}. UV−visible in CHCl$_3$, λ/nm ($\epsilon \times 10^{-4}$/M^{-1} cm^{-1}): 460(1.50); 330(16.0); 291(14.6); 268(15.8); 258(18.0).

LB Film Preparation. All LB manipulations were made in a Nima trough with a Wilhelmy balance as a surface pressure sensor. The trough was filled with ultrapure water (∼18 MΩ cm) which was purified by an EASY pure RF compact ultrapure system (Kleiner, Switzland). The trough was placed on a vibration-isolated table and the pure water subphase was thermostated by circulating the water under the trough. A chloroform solution of **1** (6.5 mg in 5 mL of chloroform), was spread onto a pure water subphase. After evaporation of the solvent for 15 min, the surface pressure−area isotherms were recorded at different subphase temperatures at a compression speed of 50 cm^2 min^{-1}. Expansions of monolayer were made at the same rate as the compressions after confirmation with no difference of the contact angle between the Wilhelmy plate and the monolayer on the water surface, immediately after the barrier hit to the surface pressures' preset. Monolayers formed on the pure water subphase were held at the constant pressures for 30 min for stabilization and were then transferred to solid supports at a rate of 5 mm min^{-1}. The films, formed at 20 ± 0.5 °C on the pure water subphase, were transferred by vertical dipping in the altered (Y-type) layered mode, namely, the substrates pre-immersed in the subphase prior to the spreading of the chloroform solution, went up and down through the interface continuously. The glass and single-crystal silicon (111) sub-strates were made hydrophilic by consecutive sonication of the substrates in detergent for 30 min and in CHCl$_3$−EtOH for 15 min, soaking in piranha solution (30%H$_2$O$_2$:concd H$_2$SO$_4$ = 1:3, v/v) for 8 h, and finally washing with copious ultrapure water. **CAUTION:** Piranha solution reacts violently, even explosively, with organic materials, and it should not be stored in sealed containers or combined with significant quantities of organic material!

Physical Measurements. UV−visible spectra of the films on glass and of a chloroform solution of the ion-pair complex were recorded on a Shimidzu UV-240 spectrometer, using blank quartz and the solvent as the references. Emission spectra were measured with a Hitachi F-4500 fluorescence spectrophotometer. Atomic force microscope (AFM) images of the monolayer films were measured on a Nanoscope IIIa AFM microscope in a tapping mode. The mica slides for AFM images were freshly cleaved immediately before use. Infrared spectra for the ion-pair complex in the LB film on CaF$_2$ substrate and in KBr pellet were recorded on a Perkin-Elmer 200-FTIR spectrophotometer. 150 nm-thick In-tin oxide (ITO) (sheet resistance of 15 Ω/square) coated glass substrates were donated by China Southern Glass Holding Co., Ltd.. Cyclic votammetry measure-ments were conducted on a model CH 600 voltammetric analyzer with an ITO substrate as working electrode, a saturated calomel electrode (SCE) as the reference electrode, and a polished platinum wire as the counter electrode. The supporting electrolyte was NaCl in water (0.5 M). Prior to each measure-ment, the solutions were deoxygenated with bubbling nitrogen for 15 min.

Results and Discussion

Surface Pressure−Area (π−A) Isotherms. The π−A isotherms of **1** at the air−water interface with different subphase temperatures of 15 °C, 20 °C, and 30 °C, are shown in Figure 2. The monolayers of **1** show subphase temperature-dependent phase transition behaviors. The shapes of π−A isotherms at each temperature are similar with a long plateau separating two regions of sharp increases in surface pressures. The plateau

surface pressures decrease with increasing the subphase temperatures: 7.1 mN m^{-1} for 15 °C, 6.3 mN m^{-1} for 20 °C, and 2.6 mN m^{-1} for 30 °C. The collapse pressures of the monolayers at the different temperatures show same temperature dependence as the plateau surface pressures: 45 mN m^{-1} for 15 °C, 34 mN m^{-1} for 20 °C, and 24 mN m^{-1} for 30 °C. Taking the isotherm at 20 °C as an example, we discuss Langmuir film-forming properties of **1** as follows: At 20 °C, the molecules on the pure water subphase give a "lifting off" area of 2.8 nm^2 molecule^{-1}; they are then compressed into a liquid expanded (LE) phase and a liquid condensed (LC) phase at 2.4−2.8 and 1.2−1.8 nm^2 molecule^{-1}, respectively. The LC phase is steeper than the LE phase, which can be seen from the slopes of the linear parts of LE phase (0.15 mN m^{-1} nm^{-2}) and the LC phase (0.93 mN m^{-1} nm^{-2}). These two slopes lie within the range of slopes for the previously reported amphiphilic lanthanide complexes,[21−26,29−31] indicating good film-forming properties of **1,** even at surface pressures below 1 mN m^{-1}. The limiting molecular areas obtained by extrapolation of the linear parts of the two phases to a zero surface pressure are found to be 2.85 and 1.75 nm^2 molecule^{-1}, respectively. On the basis of a molecular area of $A_{Ru} = \sim 1.05$ nm^2, reported for the analogous amphiphilic Ru(II) complexes of [Ru(bpy)$_2$L18]$^{2+}$ (L18 = 4,4′-dioctadecyl-carboxyl-2,2′-bipyridine) and [Ru(bpy)$_2$bpyC$_{19}$]$^{2+}$ (bpyC$_{19}$ = 4-methyl-4′-methylenestearamide-2,2′-bipyridine) on the pure water subphase[35] and $A_{Eu} = 0.62$ nm^2 for [Eu(NTA)$_4$]$^{-}$,[24] we designate the LE phase with the limiting molecular area of 2.85 nm^2 molecule^{-1} to the formation of a closely packed monolayer film. The limiting molecular area observed for this phase is 0.56 nm^2 larger than the simple summation area (2 $A_{Eu} + A_{Ru}$) of 2.29 nm^2. This difference in molecular areas is reasonable considering the packing space left and potential defects, e.g., pinholes, which may be present in the monolayer film. The difference in the limiting molecular areas for the LE and LC phases, 1.10 nm^2, cannot be ascribed to the changes in molecular conformations, e.g., the lifting off of the alkyl chain and/or the transition from a shoulder-by-shoulder to a vertically stacked (superimposed) packing of the Ru(II) complex cations and the Eu(III) complex anions caused by compression of the monolayer film from the LE phase into the LC phase. Therefore, we assign the LC phase with the limiting molecular area of 1.75 nm^2 molecule^{-1} to the formation of aggregations. To further characterize the phase properties of the monolayer film, the compression−expansion isotherms of **1** at 20 °C were measured and are shown in Figure S1 (Supporting Information). As the monolayer was compressed to a surface pressure of 6 mN m^{-1}, which is within the LE phase and was subsequently expanded, a small hysteresis was observed, characteristic of typical closely packed monolayers.[36] As the reversal surface pressure was set at 20 mN m^{-1}, which is within the LC phase, a relatively large hysteresis was observed, indicating that **1** formed aggregations on the pure water surface as compressed into the LC phase. A dramatic decreases in molecular occupied areas have been attributed to the formations of molecular aggregations at the air−water interface as reported on squaraines[37] and an amphiphilic Eu(III) complex.[21] As the monolayer was compressed to a surface pressure of over 34 mN m^{-1}, a significant hysteresis was revealed, and the monolayer could not be recovered to the pre-compression stage as the surface pressure was released to zero, showing that the monolayer collapsed as being compressed to a surface pressure over 34 mN m^{-1}.

Above all, **1** can form stable Langmuir films with a high collapse pressure on the pure water subphase without any electrolytes added. On the contrary, it was reported that [Ru-
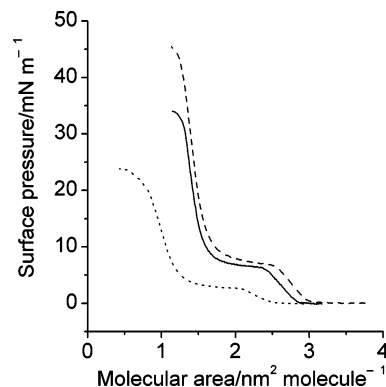

Figure 2. The surface pressure−area isotherms of **1** at the air−water interface with different temperatures of 15 °C (dashed line), 20 °C (solid line), and 30 °C (dotted line).
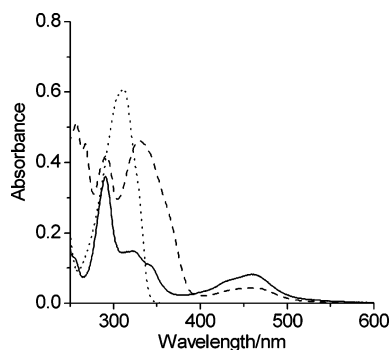

Figure 3. UV−visible spectra of L (dotted line), [Ru(bpy)$_2$L](PF$_6$)$_2$ (solid line), and **1** (dashed line) in CHCl$_3$.

(bpy)$_2$L](PF$_6$)$_2$ and some amphiphilic Ru(II) complexes exhibited continuously decreases of the surface areas upon keeping a constant film-forming surface pressure at the air−water interface in the absence of a subphase electrolyte, due to appreciable solubility of the spread molecules into the subphase water.[38]

UV−Visible Spectra. UV−visible spectra of L, [Ru(bpy)$_2$L]-(PF$_6$)$_2$ and **1** in CHCl$_3$ are compared in Figure 3. In comparison with the absorption spectra of [Ru(bpy)$_2$L](PF$_6$)$_2$ and [Eu(NTA)$_4$]$^{- \ 24}$, and with reference to the absorption spectrum of tris(bipyridyl)ruthenium(II),[39] a broad absorption band at 330 nm in the spectrum of **1** is assigned to the dominant NTA^{-1}-centered π−π* transition, and the absorption in the visible region at 460 nm is ascribed to the metal-to-ligand charge-transfer transition (^{1}MLCT), which consists of overlapping Ru-(dπ) → bpy (π*) and Ru(dπ) → L (π*) transitions. The ^{1}MLCT band shows a tail up to 550 nm, which is a 50-nm extension to lower energy compared to tris(bipyridyl)ruthenium(II),[26] indicating that the ligand L is electronically similar to 2,2′-bipyridine. The UV−visible spectra of **1** in LB films prepared at 5 and 20 mN m^{-1} are displayed in Figures 4 and 5, respectively. The spectral shapes of the LB films are independent of the surface pressures and match well with that observed in the chloroform solution with respect to both the band maxima and the relative absorption intensities of the peaks. As shown in the insets of Figures 4 and 5, the absorbance of LB films monitored at 336 and 466 nm linearly increases with the number of layers deposited, showing that **1** has good deposition behaviors at constant surface pressures lying at both the LE and the LC phases observed from the π−A curve. We have used the Beer−Lambert law modified for two-dimensional concentration, i.e., $\Gamma = 10^{-3}A/\epsilon$, where Γ is the surface concentration (mol cm^{-2}), A and ϵ are the absorbance per layer and the molar extinction coefficient for the film-forming molecule in the film at a fixed

Langmuir−Blodegett Film of Ru(II)−Eu(III) dual chromophores

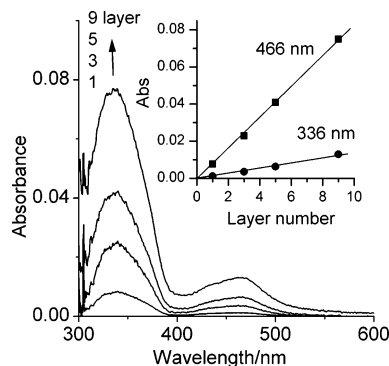*J. Phys. Chem. B, Vol. 110, No. 14, 2006* **7405**

Figure 4. The dependence of UV−visible spectra for LB films of **1** deposited at 5 mN m^{-1} on the number of layers deposited.
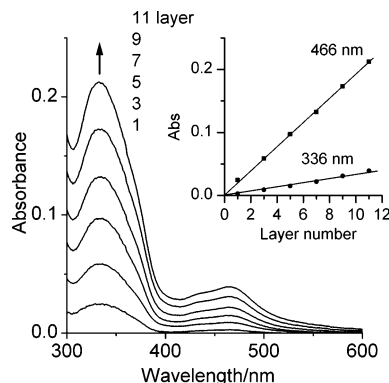

Figure 5. The dependence of UV−visible spectra for LB films of **1** deposited at 20 mN m^{-1} on the number of layers deposited.

wavelength. The absorbance per layer at 336 nm, calculated from the slopes in linear relationship for the films deposited at 5 mN m^{-1} and 20 mN m^{-1}, was found to be 0.00421/layer and 0.0096/layer, respectively. If we suppose that an ϵ value at 336 nm for **1** in the films is approximately equal to $\epsilon_{336\ nm} = 3.22 \times 10^4$ mol^{-1} dm^3 cm^{-1} for **1** in the chloroform solution, the surface concentrations of **1** in the films deposited at 5 mN m^{-1} and 20 mN m^{-1} are derived to be 1.30×10^{-10} mol cm^{-2} and 2.98×10^{-10} mol cm^{-2}, respectively. The occupied areas per molecule are derived to be 1.28 nm^2 and 2.92 nm^2 for **1** in the films deposited at 5 mN m^{-1} and 20 mN m^{-1}, respectively. The area of 2.92 nm^2 is comparable to a value of 2.85 nm^2 molecule^{-1} obtained from the π−A curve, while 1.28 nm^2 is smaller than 1.75 nm^2 molecule^{-1} obtained from the π−A curve. Although the difference is probable to be ascribed to the presence of structural defects in the film deposited at 5 mN m^{-1},[40] it is also probably due to some orientation changes of the chromophores. We also attempted to transfer the LB films at a lower surface pressure of 0.3 mN m^{-1}, but only monolayer film was deposited, the spectral feature still remained unchanged relative to the chloroform solution of **1**. However, an ITO-coated glass substrate gave poor surface concentrations of 0.86×10^{-10} mol cm^{-2} and 1.56×10^{-10} mol cm^{-2} for the films transferred at 5 mN m^{-1} and 20 mN m^{-1}, respectively, probably due to the rough surface of the ITO substrate.

Emission Spectra. The emission spectra for the solid powders of [Ru(bpy)$_2$L](PF$_6$)$_2$, HDP [Eu(NTA)$_4$] and **1**, and for monolayer LB films of **1** deposited at 0.3, 5, and 20 mN m^{-1} are compared in Figure 6. [Ru(bpy)$_2$L](PF$_6$)$_2$ gives a wide characteristic ^{3}MLCT emission band centered at 616 nm; HDP[Eu(NTA)$_4$] exhibits characteristic Eu(III) sharp emission peaks at 580, 593, 613, and 655 nm, which are due to ^{5}D$_0 \rightarrow$ ^{7}F$_j$ (j = 0, 1, 2, and 3) transitions, respectively, with the electric dipole transition (^{5}D$_0 \rightarrow$ ^{7}F$_2$) being the strongest one.[21,22] It is easy to
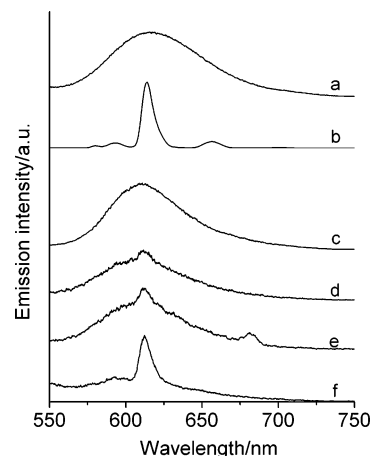

Figure 6. Emission spectra of [Ru(bpy)$_2$L](PF$_6$) powder (a, λ_{ex} = 468 nm), HDP [Eu(NTA)$_4$] in powder (b, λ_{ex} = 340 nm), **1** in powder (c, λ_{ex} = 340 nm), **1** in monolayer LB films of deposited at 20 mN m^{-1} (d, λ_{ex} = 338 nm), 5 mN m^{-1} (e, λ_{ex} = 338 nm), and 0.3 mN m^{-1} (f, λ_{ex} = 338 nm).

distinguish the dual emission from the Ru(II) and Eu(III) complexes despite the spectral overlapping observed. It is noteworthy that characteristic Ru(II) emission appears without discernible trace of Eu(III) emission in the spectrum of **1** in powder, probably due to the electron-transfer quenching of Eu-(III) emission by [Ru(bpy)$_2$L]$^{2+}$. Interestingly, the emission spectra of LB films are shown to be strongly dependent on the surface pressures used for LB depositions. For a LB film prepared at 0.3 mN m^{-1}, a dominant Eu(III) emission peak at 616 nm appears compared to the wide-band Ru(II) emission at the overlapped spectral range, sharp contrast to dominant Ru-(II) emission exhibited by **1** in power and in LB films deposited at 5 and 20 mN m^{-1}. We can also see that the emission patterns for LB films deposited at 5 and 20 mN m^{-1} are quite similar to each other with the relative intensity of Eu(III) emission at 616 nm being slightly stronger than that of Ru(II) emission at the same wavelength. In connection with reversible compression−expansion cycles of **1** at the air−water interface, as the reversal pressures were set below 6 mN m^{-1}, the LB film constitutes an Eu(III) emission switching device driven by the surface pressures, e.g., 0.3 and 5 mN m^{-1}. The emission switching observed above can be understood by the fact that the molecules of **1** are highly emissive as they are separated at a low surface pressure of 0.3 mN m^{-1}, but become highly quenched in emission as the molecules are closely packed as being deposited into the film at high surface pressures, e.g., 5 and 20 mN m^{-1}. The sensitivity in emission quenching of Eu(III) characteristic emission in LB films to the surface pressures has been observed on tris(α-thenoyltrifluoroacetonato)mono(1-octadecyl-2-(2-pyridyl)benzimidazole)europium(III).[21]

Infrared Spectra. In Figure 7, the infrared spectrum of **1** in a KBr pellet is compared with that in a 25-layer LB film transferred at 20 mN m^{-1} onto a CaF$_2$ substrate. The frequencies of CH$_2$ stretching bands are sensitive to the conformations of a hydrocarbon chain. The low frequencies of bands at 2918 and 2848 cm^{-1} are characteristic of a highly ordered alkyl chain, while their upward shifts to 2927 and 2956 cm^{-1} indicate a conformational disorder with a gauche conformations in the hydrocarbon chain.[41−44] The CH$_2$ antisymmetric and symmetric stretching frequencies for the spectrum of the KBr pellet are seen at 2924 and 2852 cm^{-1}, and are red shifted to 2918 and 2849 cm^{-1}, respectively, for the LB film, indicative of highly ordered alkyl chain in the LB film.[39] The two peaks at 1615 and 1572 cm^{-1} for the KBr pellet are assigned to the stretching
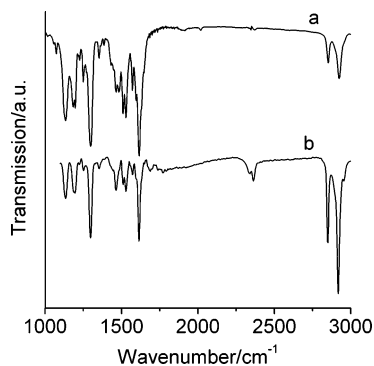
Figure 7. IR spectra for **1** in KBr pellet (a) and in a 25-layer LB film transferred at 20 mN m^{-1} onto a CaF$_2$ substrate (b).

vibration of the carbonyl groups near to and far away from the naphthalene ring,[30] respectively. The separation of these two peaks in the KBr pellet, $\Delta\nu = 33$ cm^{-1}, is identical to that observed for the LB film, and is less than a value of $\Delta\nu = 44$ cm^{-1} observed for uncoordinated free HNTA which gives the two peaks at 1672 and 1628 cm^{-1}. Also the alkenol stretching peak at 3416 cm^{-1} for free HNTA disappeared in the spectrum of **1**, indicative of deprotonation of HNTA and occurring of coordination reaction via the carbonyl oxygen atoms. These facts are in agreement with those observed previously for the ion-pair complexes composed of hemicyanines and [Ln(NTA)$_4$]$^-$ (Ln = lanthanide ion).[30] The comparisons of some characteristic peaks for the KBr pellet and the LB film (listed in brackets) are given as follows: $\nu_{(C=C)}$ at 1530 (1529) and 1509 (1510); aromatic ring stretching vibrations ν_ϕ at 1465(1465); in plane-bending vibrations of $\delta_{(C=C)} + \delta_{(C=O)}$ at 1297(1297), 1250-(1251), 1197(1198), 1185(1186), and 1133(1132) cm^{-1},[30] leading to the fact that the **1** is robust toward hydrolysis side reaction at the air−water interface.

Atomic Force Microscopy (AFM). To reveal the differences in morphologies of the monolayers at the different phases, and to get insight into the phase properties of the monolayers, an atomic force microscope study of monolayers transferred onto glass substrates at the surface pressures of 5 and 20 mN m^{-1} was carried out. As shown in Figure 8, the surface of the bare glass substrate is flat and featureless; the monolayer films deposited at 5 mN m^{-1}, on the other hand, appear as elliptical islands with a maximum length of about 0.19 μm, these islands are aggregated into larger ones with the maximum length about 0.28 μm at a higher surface pressure of 20 mN m^{-1}, and the surface of the film deposited at 20 mN m^{-1} is more corrugated than that at 5 mN m^{-1}. Atomically flat mica was also chosen for the solid supports of the monolayers in order to preserve the molecular arrangements as much as possible before and after the film transfers onto the solid support and to minimize the complication of potential phase transfers induced by the substrates.[45] Although both atomically flat mica and graphite can be used for the solid supports of the films studied by scanning probe techniques, AFM demonstrated that fatty acid molecules were induced by mica to orientate nearly vertical to the surface of the mica, while lying down when deposited on graphite.[46] The AFM images for the monolayer films transferred onto mica are shown in Figures S2 and S3 (Supporting Information). The profiles for the two images are distinctly different. The image for the monolayer film deposited at 5 mN m^{-1} is composed of flat terraces punched with many "pinholes", with a maximum diameter of about 0.5 μm. The significant defects in the film can account for the abnormally large limiting molecular area observed. The mean depth of the pinholes is 0.74 nm. This is not surprising considering the fact that the
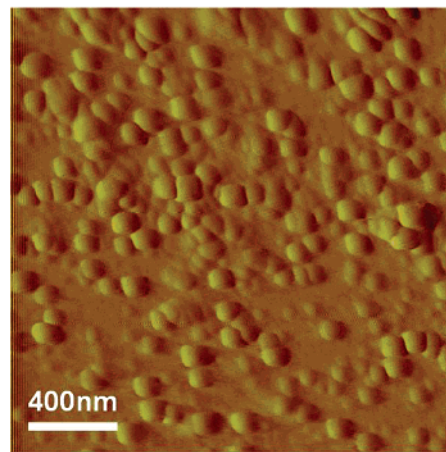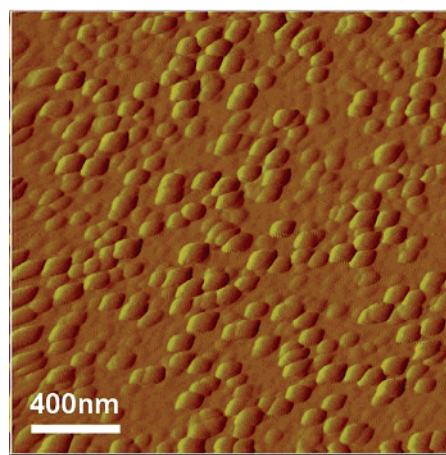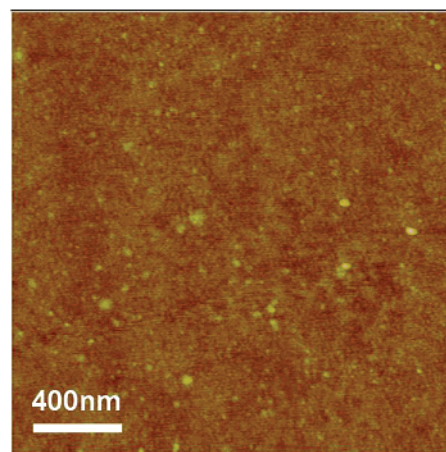

Figure 8. AFM images of bare glass substrate (top), and the monolayer films of **1** deposited at 5 mN m^{-1} (middle) and 20 mN m^{-1} (bottom).

evidently tilted long alkyl chains can easily intertwine. Upon compression of the monolayer film to 20 mN m^{-1}, the "pinholes" disappear in the AFM image instead of corrugated domains surrounded by a "moat" of mean depth of 1.16 nm. The absence of the pinholes at the higher surface pressure relative to the lower surface pressure has been observed on the LB films of Ru(L18)(tppz)(PF$_6$)$_2$ (L18 = 2,6-bis(*N*-octadecyl benziimidazolyl)pyridine; tppz = 2,3,5,6-tetrakis(2-pyridyl)-pyrazine).[47] Obviously, surface morphologies in LB monolayers of **1** can be distinctly different on hydrophilic glass and mica substrates. The surface charge of the mica plays an important role. It should be pointed out that the anionic charge of mica also likely alters the chemical composition of the films deposited, e.g., fewer [Eu(NTA)$_4$]$^-$ and more [Ru(bpy)$_2$L]$^{2+}$

Langmuir−Blodegett Film of Ru(II)−Eu(III) dual chromophores

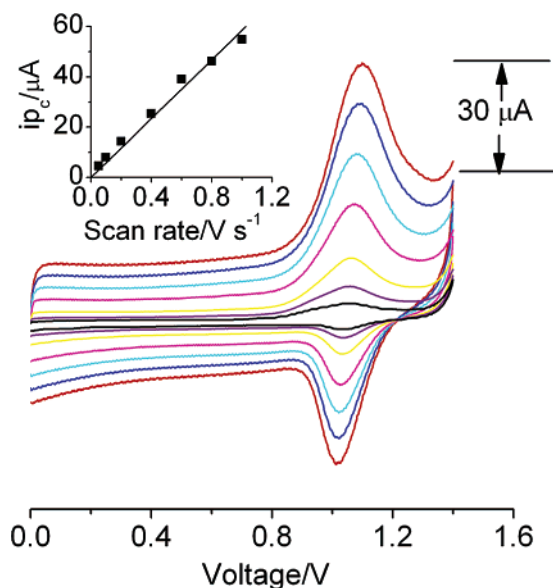*J. Phys. Chem. B, Vol. 110, No. 14, 2006* **7407**

Figure 9. Cyclic voltammograms of **1** in monolayer LB film transferred at 5 mN m^{-1}.
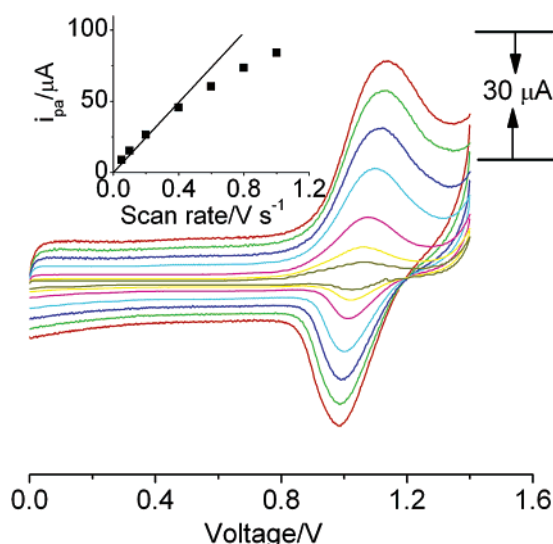

Figure 10. Cyclic voltammograms of **1** in monolayer LB film transferred at 20 mN m^{-1}.

than the 1:2 stoichiometric ratio of the Ru(II) complex cation and the Eu(III) complex anion in **1**, contributing to the difference in morphologies observed between the films on glass and mica substrates. Nanoshaving has also been done for the measurements of the thickness of the films deposited on both mica and single-crystal silicon substrates by increasing the force on the AFM tip to dig holes on the films; however, we were not able to obtain reasonable information on film thickness because of the uncertainties in the measured depths of the holes, which were caused by the contamination of the tip by the digging procedure and by piles of the molecules around the holes.[45]

Cyclic Voltammetry. The redox properties of LB films on ITO substrates were examined by cyclic voltammetry. The effects of potential scan rates on voltammograms of the monolayer LB films transferred at 5 and 20 mN m^{-1} are shown in Figures 9 and 10, respectively. The relationships between the anodic peak currents and the scan rates are exhibited in the insets of the two figures. The significantly asymmetric shapes of the redox waves were observed, indicating that the redox reaction of **1** on ITO electrode was quasi-reversible, similar to the observations on the LB film of Ru(L18)(tpy-PO$_3$H)PF$_6$,

where L18 = 2,6-bis(*N*-octadecylbenzimidazol-2-yl)pyridine and tpy-PO$_3$H = 2,2′:6′,2″-terpyridine-4′-phosphonic acid.[19] A $\Delta E_{1/2}$ (the total width at half-height of the anodic peak) value of 240 mV found for the both films transferred at 5 and 20 mN m^{-1}, is significantly larger than the Nernstian width of 90 mV.[49,50] This disagreement between the experimental and theoretical values is probably due to two reasons: (1) large intermolecular space hindrance caused the monolayer to be less ordered; therefore, all the redox centers are in a nonuniformed environment; (2) high concentration of surface-confined redox centers produce a strong lateral interaction betwen them. A formal potential $E_{1/2}$ for the anodic peak of 1.06 V found for the films deposited at 5 mN m^{-1}, is almost identical to that for the films deposited at 20 mN m^{-1}, and that observed for an analogous Ru(II) complex of [Ru(bpy)$_2$bpyC$_{19}$]$^{2+}$ (bpyC$_{19}$ = 4-methyl-4′-methylenestearamide-2,2′-bipyridine),[51] due to their similar electronic properties of L and bpyC19, but 120 mV more negative than **1** in CH$_3$CN solution ($E_{1/2}$ = 1.18 V vs SCE) (Figure S4, Supporting Information), suggesting strong interaction between the complex molecules on the ITO surface.[16] The anodic peak currents increase linearly with potential scan rates of v over scan rates of 0.05−1.0 V s^{-1} for LB films transferred at 5 mN m^{-1}, and of 0.05−0.4 V s^{-1} for LB films transferred at 20 mN m^{-1}, rather than the dependence of the anodic peak current on $v^{1/2}$ observed for **1** in CH$_3$CN solution (Figure S4), confirming the surface-confined rather than the diffuse-controlled redox reactions for the films as expected from the adsorbed redox species in a thin-layer cell according to eq 1:[48]

$$i_p = [(nF)^2 A\, \Gamma\, v]/(4RT) \tag{1}$$

where n, Γ, F, v, and A are the number of electrons involved in the electrode reaction, the surface concentration, Faraday's constant, the potential scan rate, and the electrode area, respectively. Based on this equation, the surface concentrations of **1** are found to be 1.27×10^{-10} mol cm^{-2} for the film transferred at 5 mN m^{-1} and 2.33×10^{-10} mol cm^{-2} for the film transferred at 20 mN m^{-1}. The surface concentrations of the redox-active centers on the electrode are also derived to be 0.63×10^{-10} mol cm^{-2} for the film transferred at 5 mN m^{-1}, and 1.2×10^{-10} mol cm^{-2} for the film transferred at 20 mN m^{-1} by integrating charges (Q) passing on the anodic waves at 50 mV s^{-1}, according to the following equation:[48]

$$\Gamma = Q/nFA \tag{2}$$

despite the dispencies in the surface concentrations derived from the two methods mentioned above, the surface concentrations of **1** on ITO substrate are obviously smaller than those on glass and quartz substrates, probably due to the rough surface and not as good hydrophilic properties of ITO as glass and quartz substrates. Almost no variations of cyclic voltammograms are observed after repeated successive potential scans, demonstrating that the monolayers were stable against pealing off during the potential scans. The differences between the anodic peak potential (E_{pa}) and cathodic peak potential (E_{pc}) of the immobilized Ru complex ($\Delta E_p = E_{pa} - E_{pc}$) increase with the potential scan rates, indicating that the electrode reactions are controlled by electron transfer (ET) kinetics. The ΔE_p values observed at a fixed scan rate for the film deposited at 20 mN m^{-1}, were larger than those at 5 mN m^{-1}, indicating a decrease in ET rate upon increasing film-forming surface pressures. The values of formal potential E_0 obtained as $E_0 = (E_{pa} + E_{pc})/2$, are almost the same and hardly affected by the potential scan rates, indicating that the electron-transfer coefficients for anodic

and cathodic processes are similar ($\alpha_a \approx \alpha_c = 0.5$). From observed dependence of $\Delta E_p = E_{pa} - E_{pc}$ on log ν, the standard heterogeneous electron-transfer rate constant k_s associated with the redox process of the immobilized Ru complex is estimated by using Laviron's equation:[52,53]

$$\Delta E_p = \frac{4RT}{2.303nF}\log\left(\frac{nF\nu}{2RTk_s}\right) \tag{3}$$

The k_s value for the monolayer film transferred at 5 mN m^{-1} is derived to be 0.23 s^{-1}, which is approximately 20 times the value of 9.6×10^{-3} s^{-1} for the monolayer film transferred at 20 mN m^{-1} at a fixed scan rate of 1.2 V s^{-1}. This is to say, a loosely packed film has a relatively larger k_s value than the closely packed one, as anticipated.

Conclusions

A robust and easily accessible surfactant Eu(III)−Ru(II) complex is synthesized by utilization of the europium(III) complex anion as the counterion of the amphiphilic Ru(II) complex cation. This ion-pair complex containing Eu(III) and Ru(II) complex dual chromophores, affords advantages of stable Langmuir and Langmuir−Blodgett film-forming properties as evidenced by surface pressure−area isotherm measurements and UV−visible and infrared spectroscopies. The emission spectroscopy, cyclic votammetry, and atomic force microscope studies showed that the LB films are of surface pressure-dependent emissive, interfacial electron transfer, and morphology properties. The LB films integrating dually emissive and redox centers would provide insights into developing smart photoelectric devices in the future.

Supporting Information Available: The compression−expansion isotherms at reversal pressures of 6 mN m^{-1}, 30 mN m^{-1}, and 35 mN m^{-1}, an AFM image of monolayer film of **1** deposited at 5 mN m^{-1}, an AFM image of monolayer film of **1** deposited at 20 mN m^{-1}, and cyclic voltammograms of **1** in CH$_3$CN at scan rates of 0.25−1.0 V s^{-1}. This material is available free of charge via the Internet at http://pubs.acs.org.

References and Notes

(1) Hagafieldt, A.; Grätzel, M. *Chem. Rev.* **1995**, *95*, 49.
(2) Balzani, V.; Maggi, L.; Mantrinn, M. F.; Bolletta, F.; Laurence, G. S. *Coord. Chem. Rev.* **1975**, *15*, 321.
(3) Nazeeruddin, M. K.; Rotzinger, F. P.; Comte, P.; Grätzel, M. *J. Chem. Soc., Chem. Commun.* **1988**, 872.
(4) De Silva, A. P.; Gunaratne, H. Q. N.; Gunnlaugsson, T.; Huxley, A. J. M.; McCoy, C. P.; Rademacher, J. T.; Rice, T. E. *Chem. Rev.* **1997**, *97*, 1515.
(5) Gao, F. G.; Bard, A. J. *J. Am. Chem. Soc.* **2000**, *122*, 7426.
(6) Miyashita, T.; Murakata, T.; Matsda, M. *J. Phys. Chem.* **1983**, *87*, 4529.
(7) McCullough, D. H.; Regen. S. L. *Chem. Commun.* **2004**, 2787.
(8) Ulman, A. *An Introduction to Ultrathin Organic Films, From Langmuir−Blodgett to Self-Assembly;* Academic Press: New York, 1991.
(9) DeArmond, M. K.; Fried, G. A. *Prog. Inorg. Chem.* **1997**, *44*, 97.
(10) Ferreira, M.; Wohnrath, K.; Oliveira, ON. *Synth. Met.* **2003**, *135*, 455.
(11) Haga, M.; Wang, K. Z.; Kato, N.; Monjushiro, H. *Mol. Cryst. Liq. Cryst.* **1999**, *337*, 89.
(12) Chu, B. W. K.; Yam, V. W. W. *Inorg. Chem.* **2001**, *40*, 3324.

(13) Abatti, D.; Zaniquelli, M. E.; Iamamoto, Y.; Ydemori, Y. M. *Thin Solid Films* **1997**, *310*, 296.
(14) Fukuda, N.; Mitsuishi, M.; Aoki, A.; Miyashita, T. *J. Phys. Chem. B* **2002**, *106*, 7048.
(15) Riul, A.; doc Santos, D. S.; Wohnrath, K.; Di Thommazo, R.; Carvalho, A. C. P. L. F.; Fonseca, F. J.; Oliveira, Jr., O. N.; Taylor, D. M.; Mattoso, L. H. C. *Langmuir* **2002**, *18*, 239.
(16) Okamoto, K.; Taniguchi, M.; Takahashi, M.; Yamagishi, A. *Langmuir* **2001**, *17*, 195.
(17) Santos, J. P.; Zaniquelii, M. E.; Batalini, C.; De Giovani, W. F. *J. Phys. Chem. B* **2001**, *105*, 1780.
(18) Umar, A. A.; Salleh, M. M.; Yahaya, M. *Eur. Phys. J.: Appl. Phys.* **2005**, *29*, 215.
(19) Wang, K. Z.; Haga, M. A.; Hossain, M. D.; Shindo, H.; Hasebe, K.; Honjushiro, H. *Langmuir* **2002**, *18*, 3528.
(20) Sun, M.; Xin, H.; Wang, K. Z.; Zhang, Y. A.; Jin, L. P.; Huang, C. H. *Chem. Commun.* **2003**, 702.
(21) Wang, K. Z.; Gao, L. H.; Huang, C. H. *J. Photochem. Photobiol. A. Chem.* **2003**, *156*, 39.
(22) Wang, K. Z.; Gao, L. H.; Huang, C. H.; Yao, G. Q.; Zhao, X. S.; Xia, X. H.; Xu, J. M.; Li, T. K. *Solid State Commun.* **1996**, *98*, 1075.
(23) Zhao, Y. L.; Huang, C. H.; Gan, L. B.; Ying, L. M.; Zhao, X. S.; Zhang, B.; Ma, M.; Wu, K. *Langmuir* **1998**, *14*, 417.
(24) Zhou, D. J.; Wang, K. Z.; Huang, C. H.; Xu, G. X.; Xu, L. G.; Li, T. K. *Solid State Commun.* **1995**, *93*, 167.
(25) Wang, K. Z.; Yam, V. W. W.; Huang, C. H. *Solid State Commun.* **1998**, *107*, 249.
(26) Bian, Z. Q.; Wang, K. Z.; Jin, L. P.; Huang, C. H. *Colloids Surf., A* **2005**, *257−258C*, 67.
(27) Qian, D. J.; Yang, K. Z.; Nakahara, H.; Fukuda, K. *Langmuir* **1997**, *13*, 5925.
(28) Bu, W.; Wu, L.; Zhang, X.; Tang, A. C., *J. Phys. Chem. B* **2003**, *107*, 13425.
(29) Wang, K. Z.; Huang, C. H.; Xu, G. X.; Xu, Y.; Liu, Y. Q.; Zhu, D. B.; Zhao, X. S.; Xie, X. M.; Wu, Z. Z. *Chem. Mater.* **1994**, *6*, 1986.
(30) Huang, C. H.; Wang, K. Z.; Xu, G. X.; Zhao, X. S.; Xie, X. H.; Xu, Y.; Liu, Y. Q.; Xu, L. G.; Li, T. K. *J. Phys. Chem.* **1995**, *99*, 14397.
(31) Gao, L. H.; Wang, K. Z.; Huang, C. H.; Zhao, X. S.; Xia, X. H.; Li, T. K.; Xia, X. H. *Chem. Mater.* **1995**, *7*, 251.
(32) Wang, K. Z.; Huang, C. H.; Zhou, D. J.; Xu, G. X.; Xu, Y.; Liu, Y. Q.; Zhou, D. B.; Zhao, X. S.; Xie, X. H. *Solid State Commun.* **1995**, *93*, 189.
(33) Zhou, D. J.; Huang, C. H.; Wang, K. Z.; Xu, G. X.; Zhao, X. S., Xie, X. M.; Xu, L. G.; Li, T. K. *Langmuir* **1994**, *10*, 1910.
(34) Sullian, B. P.; Salmon, D. J.; Meyer, T. J. *Inorg. Chem.* **1978**, *17*, 3334.
(35) Seefeld, K. P.; Möbius, D.; Kuhn, H. *Helv. Chim. Acta* **1977**, *8*, 2608.
(36) Wang, K. Z.; Haga, M. A.; Monjushiro, H.; Akiba, M.; Sasaki, Y. *Inorg. Chem.* **2000**, *39*, 4022.
(37) Chen, H.; Herkstroeter, W. G.; Perlstein, J.; Law, K. Y.; Whitten, D. G. *J. Phys. Chem. B* **1994**, *98*, 5138.
(38) Obeng, Y. S.; Bard, A. J. *Langmuir* **1991**, *7*, 195.
(39) Johansen, O.; Kowala, C.; Mau, A. W. H.; Sasse, W. H. F. *Aust. J. Chem.* **1979**, *32*, 1453.
(40) Torres, G. R.; Dupart, E.; Mingotaud, C.; Ravaine, S. *J. Phys. Chem. B* **2000**, *104*, 9487.
(41) Umemura, J.; Cameron, D. G.; Mantsch, H. H. *Biochim. Biophys. Acta* **1980**, *602*, 32.
(42) Sapper, H.; Cameron, D. G.; Mantsch, H. H. *Can. J. Chem.* **1981**, *59*, 2543.
(43) Maoz, R.; Sagiv, J. *J. Colloid Interface Sci.* **1984**, *100*, 465.
(44) Porter, M. D.; Bright, T. B.; Allara, D. L.; Chidsey, C. E. D. *J. Am. Chem. Soc.* **1987**, *109*, 3559.
(45) Sikes, H. D.; Woodward, J. T.; Schwartz, D. K. *J. Phys. Chem.* **1996**, *100*, 9093.
(46) Kuroda, R.; Kishi, E.; Yamano, A.; Hatanake, K. *J. Vac. Sci. Technol.* **1991**, *B9*, 1180.
(47) Haga, M. A.; Kato, N.; Honjushiro, H.; Wang, K. Z.; Hossain, M. D. *Supramol. Sci.* **1998**, *5*, 337.
(48) Bard, A. J.; Faulkner, L. R. In *Electrochemical Methods, Fundamentals and Applications;* Wiley: New York, 1980; p 522.
(49) Finklea, H. O. In *Electroanalytical Chemistry;* Bard, A. J., Rubinstein, I., Eds.; Marcel Dekker: New York, 1996.
(50) Hamann, C. H.; Hamnett, A.; Vielstich, W. *Electrochemistry;* Wiley-VCH: New York, 1998.
(51) Zhang, X.; Bard, A. J. *J. Phys. Chem.* **1988**, *92*, 5566.
(52) Laviron, E. *J. Electroanal. Chem.* **1979**, *101*, 19.
(53) Laviron, E. *Electroanalytical Chemsitry;* Bard, A. J., Ed.; Dekker: New York, 1982; Vol 12, p 53.